THE JOURNAL OF BIOLOGICAL CHEMISTRY VOL. 287, NO. 20, pp. 16424–16434, May 11, 2012
Published in the U.S.A.

Loss of Caveolin-1 Impairs Retinal Function Due to Disturbance of Subretinal Microenvironment*[S]

Received for publication, February 15, 2012 Published, JBC Papers in Press, March 26, 2012, DOI 10.1074/jbc.M112.353763

Xiaoman Li,[a] Mark E. McClellan,[a] Masaki Tanito,[b] Philippe Garteiser,[c] Rheal Towner,[c] David Bissig,[d] Bruce A. Berkowitz,[d] Steven J. Fliesler,[e,f] Michael L. Woodruff,[g] Gordon L. Fain,[g] David G. Birch,[h] M. Suhaib Khan,[i] John D. Ash,[j] and Michael H. Elliott[a,j,k1]

From the [a]Department of Ophthalmology and Dean McGee Eye Institute, [j]Department of Physiology, and [k]Oklahoma Center for Neuroscience, University of Oklahoma Health Sciences Center, Oklahoma City, Oklahoma 73104, the [b]Department of Ophthalmology, Shimane University Faculty of Medicine, Izumo, Shimane 693-8501, Japan, the [c]Advanced Magnetic Resonance Center, Oklahoma Medical Research Foundation, Oklahoma City, Oklahoma 73104, the [d]Department of Anatomy and Cell Biology, Wayne State University School of Medicine, Detroit, Michigan 48201, the [e]Research Service, Veterans Administration Western New York Healthcare System and [f]Departments of Ophthalmology and Biochemistry, University at Buffalo, State University of New York, Buffalo, New York 14215, the [g]Department of Integrative Biology and Physiology, UCLA, Los Angeles, California 90095, the [h]Retina Foundation of the Southwest, Dallas, Texas 75231, and the [i]Department of Ophthalmology, University of Florida, Gainesville, Florida 32610

Background: Caveolin-1 is widely expressed in the retina and is linked to ocular disease.
Results: Loss of caveolin-1 results in defective retinal function and ion homeostasis that is not photoreceptor-intrinsic.
Conclusion: Caveolin-1 expressed in non-neuronal cells (*e.g.* Müller glia, retinal pigment epithelium) supports neuronal function through regulating the subretinal microenvironment.
Significance: This study provides key evidence that caveolin-1 maintains retinal homeostasis.

Caveolin-1 (Cav-1), an integral component of caveolar membrane domains, is expressed in several retinal cell types, including photoreceptors, retinal vascular endothelial cells, Müller glia, and retinal pigment epithelium (RPE) cells. Recent evidence links Cav-1 to ocular diseases, including autoimmune uveitis, diabetic retinopathy, and primary open angle glaucoma, but its role in normal vision is largely undetermined. In this report, we show that ablation of Cav-1 results in reduced inner and outer retinal function as measured, *in vivo*, by electroretinography and manganese-enhanced MRI. Somewhat surprisingly, dark current and light sensitivity were normal in individual rods (recorded with suction electrode methods) from *Cav-1* knock-out (KO) mice. Although photoreceptor function was largely normal, *in vitro*, the apparent K^+ affinity of the RPE-expressed α1-Na^+/K^+-ATPase was decreased in *Cav-1* KO mice. *Cav-1* KO retinas also displayed unusually tight adhesion with the RPE, which could be resolved by brief treatment with hyperosmotic medium, suggesting alterations in outer retinal fluid homeostasis. Collectively, these findings demonstrate that reduced retinal function resulting from Cav-1 ablation is not photoreceptor-intrinsic but rather involves impaired subretinal and/or RPE ion/fluid homeostasis.

Caveolae are 50–100-nm vesicular invaginations of specialized lipid domains reported to function in lipid trafficking, in clathrin-independent endocytosis, and as signal transduction platforms (1, 2) (*e.g.* in mechanotransduction (3–5)). The inner leaflet of caveolae are coated with oligomers of 21–24-kDa integral membrane proteins called caveolins (6). Three caveolin family members (Cav-1,[2] -2, and -3) have been identified (6–8), with Cav-1 and -2 co-expressed in a number of cell types, including adipocytes, endothelial cells, and smooth muscle cells, and caveolin-3 expressed predominantly in muscle (8, 9). A variety of receptors, transporters, and signaling molecules reside within caveolae (10–12), and several of these molecules (*e.g.* nitric-oxide synthases, heterotrimeric G-proteins, and tyrosine kinases) are negatively regulated by interaction with Cav-1 (13, 14). Progress in understanding the function(s) of Cav-1 has resulted from investigations of mice in which Cav-1 has been ablated (15–18). Global deletion of Cav-1 results in loss of morphologically identifiable caveolae and a variety of abnormalities, including microvessel hyperpermeability (19), alterations in lipid metabolism (20, 21), and insulin resistance (22). Recently, dysregulation of or abnormalities in Cav-1 have been linked to diabetic retinopathy (23) and inflamed uveitic retinas (24). In addition, a frameshift mutation in Cav-1 is associated with a rare congenital lipodystrophy with severe retinitis

* This work was supported, in whole or in part, by National Institutes of Health (NIH), NEI, Grants EY019494 (to M. H. E.), EY007361 (S. J. F.), and AG034752 (D. B.); NIH, NCRR, Centers of Biomedical Research Excellence Grant RR017703; and NIH, NEI, Core Grant EY012190. This work was also supported by Oklahoma Center for the Advancement of Science and Technology Grant HR09-028, grants from the Juvenile Diabetes Research Foundation (to B. A. B.), Wayne State University School of Medicine M.D./Ph.D. program (to D. B.), and an unrestricted grant (to M. H. E. and S. J. F.) and a Sybil B. Harrington Special Scholar Award for Macular Degeneration (to M. H. E.) from Research to Prevent Blindness, Inc.

[S] This article contains supplemental Table 1 and Figs. 1–6.

[1] To whom correspondence should be addressed: Dept. of Ophthalmology, University of Oklahoma Health Sciences Center, Dean A. McGee Eye Institute, Oklahoma City, OK 73104. Tel.: 405-271-8001 (ext. 30024); Fax: 405-271-8128; E-mail: michael-elliott@ouhsc.edu.

[2] The abbreviations used are: Cav, caveolin; RPE, retinal pigment epithelium; ERG, electroretinography; MEMRI, manganese-enhanced magnetic resonance imaging; IR, inner retina; OR, outer retina; ERG, electroretinography; cd, candela; Td, troland.

pigmentosa-like ocular abnormalities (25). Most recently, common variants near the *CAV1* locus have been associated with increased risk of primary open angle glaucoma (26, 27).

Caveolin-1 is expressed in several retinal cell types: photoreceptors (28–33), retinal pigment epithelium (RPE) (34–36), Müller glial cells (37, 38), and retinal vascular endothelium (39–43). In photoreceptors, several phototransduction proteins, including transducin, RGS-9, arrestin, guanylate cyclase, rhodopsin kinase, and the cyclic nucleotide-gated channel, cofractionate in Cav-1-enriched membranes (32, 33, 44), and Cav-1 and the α-subunit of transducin co-immunoprecipitate in a cholesterol- and guanine nucleotide-dependent manner (30). Recently, Cav-1 has been identified as a component of photoreceptor disks (29), and the disk-localized protein, Rom-1, is associated with Cav-1-enriched membranes from disks (28). Little is known about the role that Cav-1 and/or caveolae play in the posterior retina (*e.g.* photoreceptors and RPE). In RPE cells, caveolae exhibit a unique bipolar distribution (35), but their functions in either the apical or basolateral RPE membrane domains have not been elucidated.

In this report, we investigated the effects of global deletion of Cav-1 on retinal function and structure. Our data indicate that ablation of Cav-1 results in reduced outer retinal function that is not intrinsic to the photoreceptors *per se* but rather is due to a disturbance of the subretinal/RPE microenvironment.

EXPERIMENTAL PROCEDURES

Reagents—Sodium cacodylate, 50% glutaraldehyde, and 20% formaldehyde were purchased from Ladd Research Industries (Williston, VT). Rabbit polyclonal antibodies against PDE6α and arrestin and mouse monoclonal antibody against rhodopsin (RET-P1) were purchased from Thermo Scientific (Rockford, IL). Rabbit polyclonal antibodies against Transducin α and β were obtained from Santa Cruz Biotechnology, Inc. (Santa Cruz, CA). Rabbit polyclonal antibody against Caveolin-1 was purchased from BD Biosciences. The monoclonal antibody (a6F) against the α1-subunit of the Na^+/K^+-ATPase developed by Douglas Fambrough was obtained from the Developmental Studies Hybridoma Bank developed under the auspices of the NICHD, National Institutes of Health, and maintained by the University of Iowa (Iowa City, IA). All other reagents were from Sigma-Aldrich or Thermo Scientific.

Animals—All procedures were carried out according to the Association for Research in Vision and Ophthalmology Statement for the Use of Animals in Ophthalmic and Vision Research and were approved by Institutional Animal Care and Use Committees of the University of Oklahoma Health Sciences Center, Oklahoma Medical Research Foundation, and the Dean A. McGee Eye Institute. Experiments were performed on *Cav-1* KO mice (17) on either a C57BL/6J or C57BL/6J/129 background. C57BL/6J and C57BL/6J/129 F2 mice were used as controls for individual strains, respectively.

Electroretinography—Electroretinograms were recorded as described previously (45) with slight modification. Briefly 8-week-old mice were dark-adapted overnight and then deeply anesthetized under dim red light by intraperitoneal injection of a combination of ketamine (80 mg/kg) and xylazine (5 mg/kg). Pupils were dilated with 0.5% atropine and 2.5% phenylephrine, and gold wire electrodes were placed centrally on the cornea. A reference electrode was placed in the mouth, and a ground electrode was placed on the tail. To assess rod-driven retinal function, increasing scotopic stimuli (0.4–3.4 log scotopic troland (Td)·s/m^2) were presented in 0.3 log steps using a Colordome Espion electroretinography (ERG) recording system (Diagnosys, Lowell, MA). For better determination of rod-driven *b*-wave amplitudes, some mice were presented with weaker flash stimuli as well (−2.2 to −0.15 log scotopic Td·s/m^2). To assess the effect of *Cav-1* deletion on rod phototransduction, *in vivo*, the leading edge of the *a*-wave was fit by a computational model of phototransduction activation (46) using Matlab® software (MathWorks, Natick, MA). This model is described by the equation, $P3(i,t) = (1 - \exp(-1/2 \cdot i \cdot S \cdot (t - t_d)^2)) \cdot Rm_{P3}$ for $t \geq t_d$, where S is a sensitivity parameter (an indicator of phototransduction gain) that scales the flash energy, i. Rm_{P3} is the maximum *a*-wave amplitude, and t_d is a brief delay.

Possible defects in the visual cycle were analyzed by measuring the time course of recovery of rod photoreceptor sensitivity following a bleaching light exposure (47). WT and *Cav-1* KO mice were dark-adapted for a minimum of 12 h and anesthetized, and pupils were dilated as described above. Full-field scotopic ERGs were recorded for both eyes. A single test flash of 2.3 log cd·s/m^2 was presented to elicit saturated rod *a*-wave response under fully dark-adapted conditions. Mice were then exposed to steady illumination at 2.7 log cd/m^2 for 5 min in the Ganzfeld dome to bleach rod photoreceptors. Immediately following the bleaching period (time = 0 min) and every 10 min thereafter (time = 10, 20, 30, 40, and 50 min), the same test flash of 2.3 log cd·s/m^2 was presented. The *a*-wave responses at the indicated times after bleaching were normalized to the initial dark-adapted response for each mouse.

Manganese-enhanced MRI (MEMRI)—Cav-1 KO and control mice were dark-adapted overnight, injected with $MnCl_2$ (66 mg/kg intraperitoneally) under dim red light, and maintained in darkness for 4 h prior to preparation for MRI measurements, as described previously (48, 49). All animal manipulations, including MRI examination, were performed under dim red light. Mice were anesthetized with isoflurane (2–3%) and positioned laterally in the imaging cradle. MRI was carried out on a 7T Bruker Biospec system (Bruker, Ettlingen, Germany) equipped with a 300-millitesla/m gradient set, and a 1-cm single loop transmit/receive surface coil, positioned immediately above the left eye. A three-dimensional RARE sequence (multi-echo train spin echo) was used with sinc waveforms for radiofrequency excitation and refocusing and a repetition time of 400 ms. A coil spatial sensitivity profile was adjusted by tailoring pulse amplifier gains on a per animal basis. A square field of view of 12.8 × 12.8 mm^2 ranging over seven contiguous 620-μm axial slices was used and covered with a 512 × 512-element matrix, resulting in a 25 μm in-plane resolution. Acquisition time was 1 h.

For analysis of layer-specific signal intensities, central retinal signal intensities were first extracted from each image using the program NIH Image and derived macros (50), and the results from that group were compared using a generalized estimating equation approach (51) (described below). Changes in receiver gain among animals were controlled for by setting the signal

intensity of a fixed region of noise in each mouse to a fixed value, as described previously (48, 49). Post-receptor (or inner retina (IR)) and receptor (or outer retina (OR)) signal intensity data (from 0.4 to 1 mm from the center of the optic nerve) were extracted as follows. As we have previously discussed, under these conditions, the IR/OR division is not observable in dark-adapted retinas (51). To ensure that we are measuring from IR and OR, regions 3 pixels posterior to the retina/vitreous border and 4 pixels anterior to the retina/sclera border (both borders are easily observed) were analyzed to sample the IR and OR, respectively, as described previously (51). To measure retinal thickness, we used in-house written software to first map the *in situ* image into a linear representation for each retina, as described previously (52). The linearized data from each hemiretina between 0.4 and 1 mm from the optic nerve were binned. For each bin, the average profile of signal intensity as a function of retinal depth was calculated, and the vitreous-retina and retina-choroid borders were found using the "half-height" method (53). The distance between these two borders is the whole retinal thickness.

Suction Electrode Recordings of Single Rods—Methods for recording responses of mouse rods have been given previously (54, 55). *Cav-1* KO and control mice were dark-adapted for at least 3 h in a light-tight box. Animals were sacrificed, and eyes were removed under dim red light. The retinas were dissected and finely chopped in Locke's solution (140 mM NaCl, 3.6 mM KCl, 2.4 mM $MgCl_2$, 1.2 mM $CaCl_2$, 10 mM glucose, 3 mM HEPES, 5 mM sodium ascorbate, 0.02 mM EDTA, pH 7.4) using infrared illumination and a dissection scope equipped with an infrared-sensitive camera cabled to a TV monitor. The retinal pieces were pipetted onto the stage of an inverted microscope for suction recording. Rods were perfused at 37–39 °C with Dulbecco's modified Eagle's medium (D-2902, Sigma), supplemented with 15 mM $NaHCO_3$, 2 mM sodium succinate, 0.5 mM sodium glutamate, 2 mM sodium gluconate, and 5 mM NaCl. Responses recorded by an Axonpatch 200A were filtered at 30 Hz (8-pole, Bessel) and sampled at 100 Hz. Flashes of 500-nm light 20 ms in duration were attenuated to different light levels by absorptive neutral density filters. The current traces shown in Fig. 4, *A* and *B*, were average responses to 10–20 flashes for the dim lights, 5–10 flashes for the medium lights, and 3–5 flashes for the saturating lights. The time in saturation was measured as the time from the beginning of the flash to the time at which the mean circulating current returned to 25% of the dark-adapted value. Flash sensitivities were calculated by dividing the peak amplitude of the mean dim flash response for each cell by the flash intensity.

Immunohistochemistry and Confocal Microscopy—Immunohistochemistry was performed as described previously with some modification (56). Briefly, mice were killed by CO_2 inhalation, eyes were removed, cornea were dissected away, and resulting eyecups were fixed for 30 min with 4% paraformaldehyde in 0.1 M sodium phosphate (pH 7.5) and cryopreserved by sequential sucrose incubation. Tissues were embedded in OCT medium, and 8–15-μm sections were cut and mounted on slides. Slides were dipped in −20 °C methanol, air-dried, and stored at −20 °C. For immunostaining, sections were blocked for 1 h at room temperature with 10% normal horse serum in PBS supplemented with either 0.1% Triton X-100 or saponin and then incubated overnight at 4 °C with rabbit polyclonal anti-Cav-1 (1:400), mouse monoclonal anti-α1-Na^+/K^+-ATPase (a6f; 1:100), and/or mouse monoclonal anti-rhodopsin (RETP1; 1:1000). Slides were washed with PBS, incubated with Alexa Fluor-conjugated secondary antibodies (Alexa Fluor-488 and -594, Invitrogen), stained with DAPI, and imaged on an Olympus Fluoview FV500 confocal microscope.

Morphometric Analysis—Morphometry was performed as described previously (45) on tissues fixed with Perfix (20% isopropyl alcohol, 2% trichloroacetic acid, 4% paraformaldehyde, and 2% zinc chloride) and embedded in paraffin. Sections (5 μm) containing the retina, including the optic disc, were cut along the vertical meridian of each eyeball and stained with hematoxylin and eosin. For each section, digitized images of the entire retina were captured using a Nikon E800 digital imaging system (Nikon, Tokyo, Japan). The outer nuclear layer thickness was measured at 0.25, 0.75, 1.25, and 1.75 μm superior and inferior to the optic nerve head and at the periphery 100 mm from the inferior and superior edges of the retina, using ImageJ 1.32j software (available from the National Institutes of Health Web site) that was developed by Wayne Rasband. Thickness values obtained from the right and left eyes were averaged for each animal.

Conventional Electron Microscopy—Eyes from WT and Cav-1 KO mice were removed, a slit was cut in the cornea, and the eyes were placed in fixative (0.1 M sodium cacodylate buffer (pH 7.4) containing 2.5% glutaraldehyde, 2.0% formaldehyde, and 0.025% $CaCl_2$). Eyes were processed for conventional EM as described previously (57).

Retinal Adhesion Assay—This assay was developed by the Finnemann laboratory (58) and provides a simple and quantitative measure of melanin adhesion to the retinal surface. Eyecups with retinas intact were incubated at room temperature for 10 min in normosmotic or hyperosmotic Hanks' balanced salt solution (supplemented with 600 mM sorbitol), eyecups were flattened, and retina were carefully peeled from the RPE surface with fine forceps. The retinas were then solubilized in STE buffer (10 mM Tris-HCl, pH 7.4, 150 mM NaCl, 1 mM EDTA) containing 60 mM octyl glucoside, 1% Triton X-100, and protease inhibitor mixture. Lysates were centrifuged at 16,000 × *g* to pellet insoluble melanin pigment. The protein content of detergent-soluble lysates was determined by BCA assay and used to normalize the pigment content for each sample. The detergent-insoluble pellet containing melanin was washed with chloroform/MeOH (1:1) and dried, and melanin was dissolved in 20% DMSO, 2 N NaOH at 65 °C. Absorbance of dissolved pigment was read at 490 nm and compared with a standard curve of commercial melanin (Sigma-Aldrich).

Na^+/K^+-ATPase Activity—Microsomal membranes were prepared from mouse eyecups from which retinas had been carefully removed after brief incubation under hyperosmotic conditions. Membranes were fractionated on discontinuous sucrose density gradients (32, 42, and 47% sucrose in 10 mM Tris-HCl (pH 7.4)) centrifuged at 100,000 × *g* for 1 h at 4 °C. Membranes enriched in the α1-subunit of the Na^+/K^+-ATPase were collected at the 32/42% sucrose density interface, diluted

with 10 mM Tris-HCl (pH 7.4) buffer, and centrifuged at 100,000 × *g* to concentrate membranes. Membrane pellets were then resuspended in the same buffer, and protein content was determined by the BCA method.

Na^+/K^+-ATPase was partially purified from eyecup microsomes by extraction with 0.1% SDS buffered with 1% bovine serum albumin using a modification (59) of the method of Jorgensen (60). Na^+/K^+-ATPase activity was measured as a function of $[Na^+]$ (0–100 mM with $[K^+]$ fixed at 26 mM) or $[K^+]$ (0–26 mM with $[Na^+]$ fixed at 100 mM) in reaction buffer containing 50 mM Tris-HCl (pH 7.4), 3 mM $MgCl_2$ in the presence or absence of 1 mM ouabain. The reaction is initiated by the addition of 3 mM ATP (Tris-salt) and allowed to proceed for 20 min at 37 °C. ATP hydrolysis was assayed by the colorimetric Fiske-Subbarow (61) determination of released P_i by the method of Forbush (59) as modified by Cariani *et al.* (62) to use bismuth citrate instead of sodium arsenite as a molybdate chelator. Under these conditions with this amount of protein (0.5 μg/reaction), the assay was linear, and ATP remained saturating. The apparent K^+ and Na^+ affinities were calculated by fitting the K^+ and Na^+ activation curves to the Hill equation for ligand binding using GraphPad Prism 5® software (GraphPad Software, San Diego, CA).

Preparation of Rod Outer Segments—For each rod outer segment preparation, six retinas were pooled from three mice. Rod outer segments were isolated by discontinuous sucrose density centrifugation as described (45). Purity was evaluated by SDS-PAGE.

SDS-PAGE and Western Blotting—Protein content was determined by the BCA assay (Pierce) using bovine serum albumin as a standard. Equal amounts of protein were loaded on 4–20% Tris-glycine gels (Invitrogen) for electrophoresis. For direct visualization, gels were stained with Gelcode blue staining reagent (Thermo Scientific). For Western blots, proteins were transferred to nitrocellulose membranes and then probed with the indicated antibodies. Primary antibodies and dilutions used were as follows: mouse monoclonal anti-α1-Na^+/K^+-ATPase (a6f; 1:1000) and rabbit polyclonal antibodies against Cav-1 (1:2000), PDE6α (1:1000), arrestin (1:1000), and transducin subunits (1:4000). Immunoreactivity was detected using horseradish peroxidase-conjugated secondaries and imaged on an Eastman Kodak Co. Image System In Vivo F-Pro (Carestream Health, Inc., Rochester, NY).

Rhodopsin Assay—Rhodopsin measurements were performed as described previously (45, 47) with slight modification. Briefly, under dim red light, each retina was homogenized in 100 μl of buffer containing 10 mM Tris-HCl (pH 7.4), 150 mM NaCl, 1 mM EDTA, 2% (w/v) octyl glucoside, and 50 mM hydroxylamine. Homogenates were centrifuged at 16,000 × *g*, and soluble lysates were scanned from 270 to 800 nm in a spectrophotometer (Ultrospec 3000 UV-visible spectrophotometer, GE Healthcare). Samples were then bleached under room light for 10 min and scanned again. The difference spectra at 500 nm between pre- and postbleached samples were used to determine rhodopsin content using a molar extinction coefficient of 42,000 M^{-1} (63). The values were normalized to the total lysate volume and presented as rhodopsin content/retina.

Lipid Analysis—Analyses of cholesterol and fatty acids were performed essentially as described previously (44, 64) using a two-part extraction procedure to separate saponifiable from nonsaponifiable lipids. Briefly, samples were supplemented with internal standards (19-hydroxycholesterol (Steraloids, Inc., Newport, RI) and 15:0, 17:0, and 21:0 fatty acid standards (Nu-Chek Prep, Elysian, MN)) prior to saponification with 2% (w/v) KOH in ethanol at 100 °C for 1 h. Distilled H_2O (3 ml) was added, the nonsaponifiable lipids were extracted three times into hexane, and the recovered organic phases were pooled. The aqueous phase was acidified by the addition of 200 μl of concentrated HCl and sonicated for 10 min prior to extraction three times into hexane (this organic phase contains saponified fatty acids). Both saponifiable and nonsaponifiable lipid extracts were dried under N_2, and the nonsaponifiable lipids were resuspended in 50 μl of methanol for HPLC injection. Cholesterol was separated on a C18 column (Supelcosil LC-18, 25 cm × 4.6 mm, 5-μm particle size) with an isocratic mobile phase of 1 ml/min methanol. Detection was at 208 nm using an Agilent1100 series photodiode array detector; cholesterol was quantified based upon absorbance at 208 nm, in comparison with an authentic cholesterol standard (within the linear response range), and corrected for recovery of the 19-hydroxycholesterol internal standard. The fatty acid extract was analyzed as described previously (65).

Statistical Analyses—Analysis of variance with post hoc Neuman-Keuls test and *t* tests was performed using GraphPad Prism 5 software. Statistical analyses of suction electrode measurements were done with the program Origin (Microcal, Northampton, MA). Comparisons of MEMRI retinal signal intensities were performed with a generalized estimating equation approach. The generalized estimating equation performs a general linear regression analysis using all of the pixels in each subject and accounts for the within-subject correlation between adjacent pixels (48, 49). An analysis of variance-type generalized estimating equation test is not readily available. Instead, exact *p* values from two-tailed comparisons are provided. When the *p* values are very low (*e.g.* $p = 0.0001$), the likelihood of false rejection of a true null in multiple comparisons is very small. *p* values of ≤0.05 were considered significant.

RESULTS

Cav-1 Ablation Results in Reduced Retinal Function—As shown in Fig. 1, Cav-1 is expressed throughout the mouse retina with prominent expression in Müller glia, retinal, and choroidal vasculature and RPE. Weak immunoreactivity was also observed in photoreceptor inner segments. In the outer retina (outer nuclear layer and outer plexiform layer), Cav-1 immunoreactivity is more intense. At the resolution of confocal microscopy, we are unsure if this immunoreactivity is derived solely from Müller glial cells or also from expression in photoreceptors because it is expressed in both cell types albeit enriched in the former (37, 38). Based on localization in the outer retina, cofractionation with phototransduction proteins (32, 33, 44), and interaction, *in vitro*, with transducin α-subunits (30), we hypothesized that loss of Cav-1 might affect retinal function. Therefore, we assessed retinal light responses in

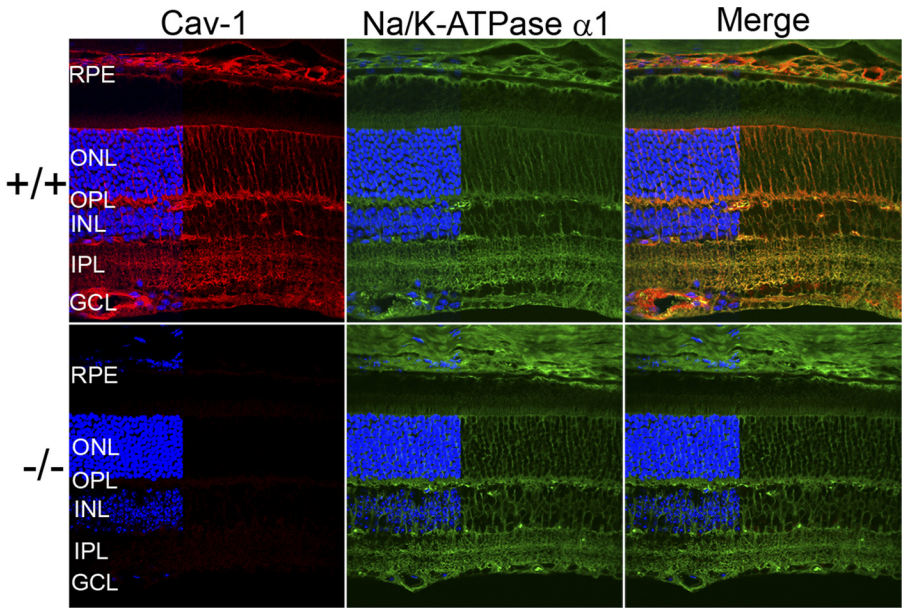

FIGURE 1. **Localization of Cav-1 in the mouse retina.** Cav-1 immunoreactivity (*red*, *left panels*) is predominantly localized to Müller glia and to retinal and choroidal vascular cells with weaker labeling apparent in the RPE. The α1 isoform of Na^+/K^+-ATPase (*green*, *middle panels*) partially colocalizes with Cav-1 in Müller glia and in the apical RPE. Loss of Cav-1 does not result in obvious changes in Na^+/K^+-ATPase localization (*green*, *middle panels*). DAPI staining (*blue*), which labels retinal cell nuclei is indicated to the *left* of each *panel* to delineate the positions of retinal layers. The *blue* channel was partially removed from the images by Photoshop in order to clearly observe Cav-1 and Na^+/K^+-ATPase localizations in retinal nuclear layers. *ONL*, outer nuclear layer; *OPL*, outer plexiform layer; *INL*, inner nuclear layer; *IPL*, inner plexiform layer; *GCL*, ganglion cell layer.

Cav-1 KO mice, *in vivo*, by ERG and MEMRI (see below). *Cav-1* KO mice displayed significant decreases in *a*- and *b*-wave amplitudes across a range of flash intensities when compared with control mice (Fig. 2, *A* and *B*). To assess rod function in greater detail, a subset of mice ($n = 5$) was analyzed by fitting the leading edge of the rod-driven *a*-wave to a computational model of phototransduction (46, 66) (supplemental Fig. 1, *A* and *B*). The algorithm allowed us to calculate maximal *a*-wave amplitude (Rm_{p3}) and sensitivity (log *S*), a measure of the amplification of phototransduction. The Rm_{p3} and log *S* were 373.0 ± 71.56 μV and 2.37 ± 0.14 s^{-2} $(Td/s)^{-1}$, respectively, in WT and 159.8 ± 57.62 μV and 1.28 ± 0.43 s^{-2} $(Td/s)^{-1}$ in Cav-1 KO. The reduction in both Rm_{p3} and log *S* in *Cav-1* KO mice suggested a defect in phototransduction.

MEMRI Revealed Evidence for Dark Current Generation in Cav-1 KO Mice—In darkness, rod photoreceptors maintain a steady inward current (the "dark current") through open nonselective cyclic nucleotide-gated cation channels (67). The function of these channels can be assessed, *in vivo*, by measuring the uptake of Mn^{2+} (a strong MRI contrast agent that is an analog to Ca^{2+}) in the outer retinal (photoreceptor) layer by MEMRI (51). MEMRI also simultaneously measures ion uptake in inner retinal neurons. We measured intraretinal Mn^{2+} uptake in *Cav-1* KO and control mice under dark-adapted conditions. As shown in Fig. 3, ion uptake in the outer retina was significantly suppressed in *Cav-1* KO mice compared with controls, suggesting that the dark current was reduced in *Cav-1* KO mice; inner retinal uptake was also subnormal. Such reductions in dark current could explain the reduced ERG *a*-wave response amplitudes observed in *Cav-1* KO mice. Outer retinal ion uptake has been shown to be suppressed when the regeneration of rhodopsin by the visual cycle is inhibited (68). However, our results suggest that this is unlikely to explain the reduced outer retinal ion uptake observed in *Cav-1* KO retinas because dark adaptation rates determined by the recovery of *a*-wave responses after photobleaching (supplemental Fig. 4) and the content of fully dark-adapted rhodopsin (supplemental Fig. 3*C*) were not different between *Cav-1* KO and control mice.

Reduced Function in Cav-1 KO Mice Did Not Result from Alterations in Photoreceptor Structure or Biochemistry—We hypothesized that the ERG phenotype observed in *Cav-1* KO mice might result from gross changes in photoreceptor structure or biochemistry. Therefore, we assessed photoreceptor morphology by light and electron microscopy. As shown in supplemental Fig. 2, *A–E*, no significant differences in retinal morphology or in photoreceptor outer nuclear layer thickness (a quantitative measure of photoreceptor numbers) were observed between *Cav-1* KO and control mice. This indicated that the reduced function measured by ERG and MEMRI was not the result of a loss of photoreceptor cells. Furthermore, no significant differences in total retinal thickness were observed when measured *in vivo* by MRI (201 ± 6 μm *versus* 199 ± 9 μm; control *versus Cav-1* KO, respectively, $n = 8$). The ultrastructure of *Cav-1* KO photoreceptors was also normal with well developed outer segment and disks (supplemental Fig. 2, *F* and *G*). We next examined several aspects of photoreceptor biochemistry, including rod outer segment protein composition (supplemental Fig. 3*A*), levels of phototransduction proteins (supplemental Fig. 3*B*), and levels (supplemental Fig. 3*C*) and localization of rhodopsin (supplemental Fig. 3*D*). Because Cav-1 is implicated in lipid trafficking, we also examined rod outer segment lipid composition. We found no differences in fatty acid composition (supplemental Table 1) or cholesterol content between *Cav-1* KO and control outer segment membranes (cholesterol/phospholipid molar ratios = 0.14 ± 0.02

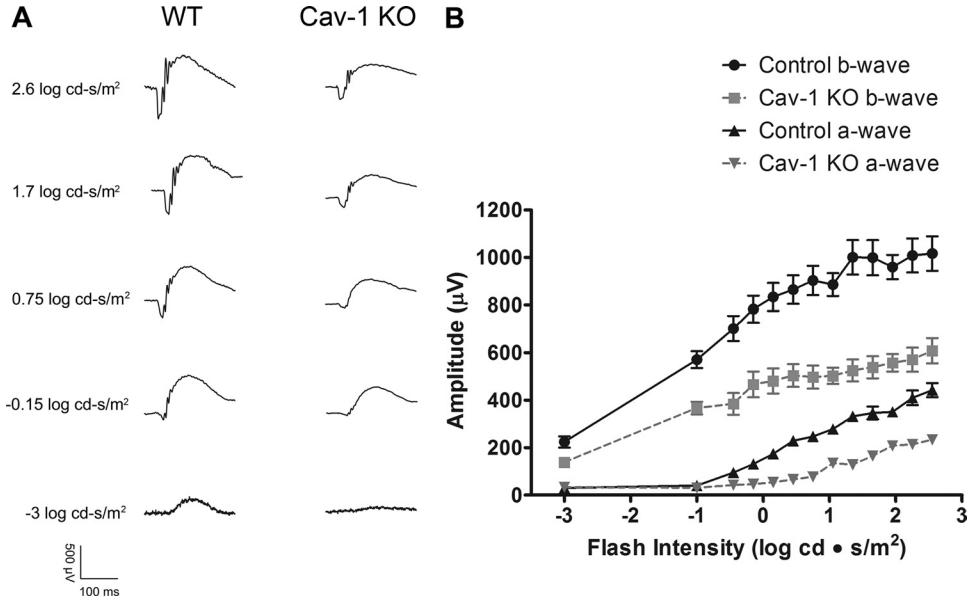

FIGURE 2. **Reduced retinal function in *Cav-1* KO mice.** Retinal function was assessed by recording ERG responses to flashes of light of increasing intensities. *A*, representative ERG responses from control and *Cav-1* KO to flashes with intensities of −3, −1.5, −0.75, 1.7, and 2.6 log cd·s/m^2 are shown. *B*, intensity/response relationships showed reductions in both *a*-wave and *b*-wave amplitudes for *Cav-1* KO mice compared with controls. Data points represent the mean ± S.E. (*error bars*) for at least 25 mice/group.

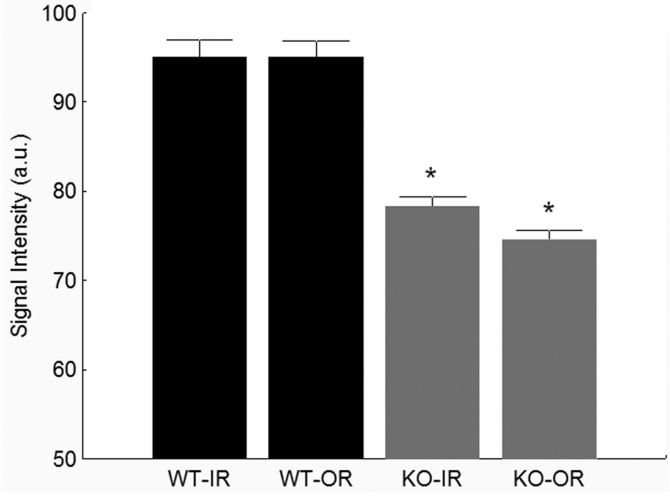

FIGURE 3. **Cav-1 KO mice showed reduced ion uptake as measured by functional MRI.** MEMRI signal intensity (arbitrary units (*a.u.*)) reduced in both IR and OR in dark-adapted *Cav-1* KO mice compared with control measured 4 h after intraperitoneal systemic administration of $MnCl_2$. *, $p < 0.05$. *Bars* represent mean ± S.E. (*error bars*) for $n = 5$ mice/group.

versus 0.13 ± 0.01; Cav-1 KO *versus* control, respectively; $n = 3$ independent membrane preparations). Collectively, these results clearly indicate that reduced retinal function cannot be explained by gross changes in photoreceptor structure or composition.

Normal Dark Current and Photoresponses in Isolated Cav-1 KO Rods—The subnormal ERG and MEMRI responses led us to speculate that rod phototransduction might be impaired. Therefore, response properties from *Cav-1* KO and control rods were recorded by suction electrode methods (55, 69). Interestingly, *Cav-1* KO rods displayed a normal circulating current and normal suppression of this current by light (Fig. 4, *A* and *B*) with normal sensitivity (0.26 ± 0.03 *versus* 0.31 ± 0.02 pA/photon/μm^2 for Cav-1 KO *versus* control, respectively; also see supplemental Fig. 5*A*). The times in saturation were reduced slightly (supplemental Fig. 5*B*), but there was no change in slope of time in saturation *versus* light intensity, indicating that the dominant time constant for response recovery (Pepperberg constant) was not significantly influenced by the absence of Cav-1. The single photon responses were somewhat sluggish in Cav-1 KO rods (supplemental Fig. 5, *C* and *D*) and showed a reduced integration time for the dim light responses, but these reduced kinetic parameters cannot account for the functional deficits observed by ERG and MEMRI. Taken together, these data indicate that the visual deficits in *Cav-1* KO mice were not photoreceptor-intrinsic. Because suction electrode recordings are carried out under conditions in which the extracellular medium is controlled, the results suggest that loss of Cav-1 results in alterations in the photoreceptor microenvironment *in situ*.

Abnormal Retinal Adhesion in Cav-1 KO Retinas—Alterations in outer retinal ion and fluid homeostasis have been shown to influence retina/RPE adhesion *ex vivo* (70). In the course of our biochemical analyses of *Cav-1* KO retinas, we also observed enhanced adhesion of RPE pigment to the surface of dissected retinas when peeled from the RPE (Fig. 5*A*). In many cases, the adherent pigmented material on the retinal surface retained the characteristic hexagonal shape of RPE cells. Immunohistochemical analyses of eyecups after peeling the retina using apical RPE markers suggested that only the apical surface of the RPE was adhering (data not shown). To quantify this enhanced adhesion, we measured the levels of melanin pigment adherent to the retinas as described previously (58). Melanin content was significantly increased in retinas from *Cav-1* KO mice (Fig. 5*B*). Interestingly, when eyecups were incubated in hyperosmotic medium (Hank's balanced salt solution with 600 mM sorbitol), retinal adhesion in *Cav-1* KO mice was significantly reduced (Fig. 5*B*). This intriguing finding is strikingly

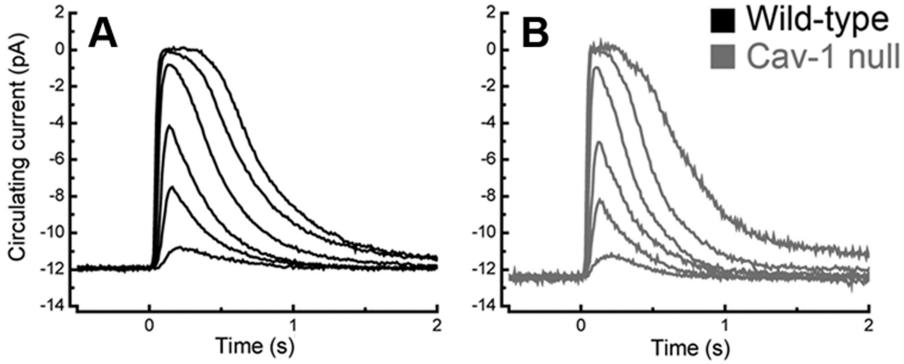

FIGURE 4. **Suction electrode recordings of rod light responses to graded series of in WT and *Cav-1* KO mice.** *A*, mean current traces in WT rods to flashes at intensities of 4, 17, 43, 160, 450, and 1122 photons μm^{-2}. The average dark current in WT rods was 14.1 ± 0.6 pA ($n = 45$). *B*, mean current traces from *Cav-1* KO rods to the same flash intensities. The average dark current in *Cav-1* KO rods was 12.5 ± 1.1 pA ($n = 9$), not significantly different from WT ($p = 0.24$, Student's *t* test). The flash sensitivity of the *Cav-1* rods was 0.26 ± 0.03 pA/photon/μm^2 ($n = 9$), not significantly different ($p = 0.20$) from WT (0.31 ± 0.02 pA/photon/μm^2; $n = 45$). For more details about suction electrode-determined parameters, see "Experimental Procedures" and supplemental Fig. 5.

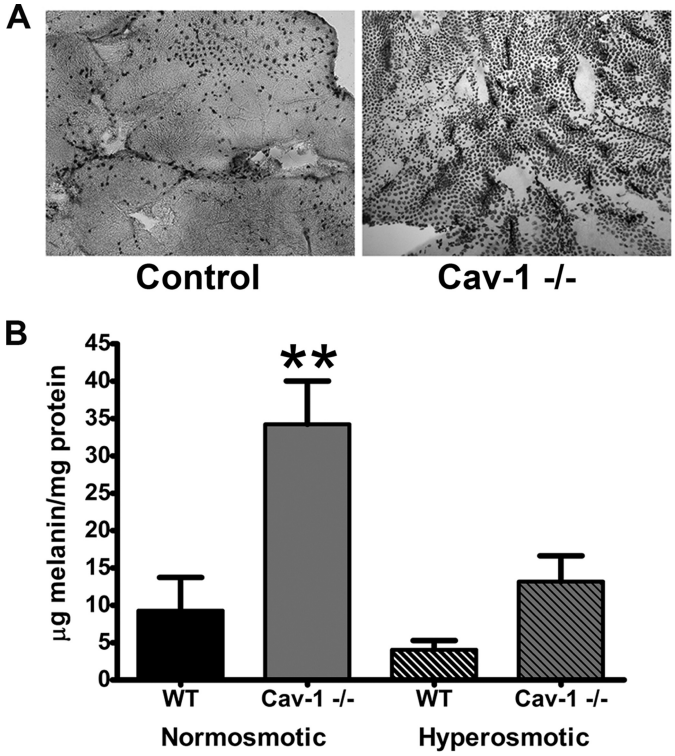

FIGURE 5. **Enhanced retinal adhesion in *Cav-1* KO mice.** *A*, increased adhesion of RPE to retinal surface was observed qualitatively in *Cav-1* KO retina flat mounts compared with controls. The amount of adherent melanin was quantified (*B*) in retinal extracts as described under "Experimental Procedures." *B*, melanin content in *Cav-1* KO retinas was significantly higher than normosmotic controls. Incubation with hyperosmotic medium resulted in a significant reduction in adherent melanin to *Cav-1* KO retinas. **, significant differences between normosmotic *Cav-1* KO and all other groups, $p \leq 0.05$; analysis of variance with Tukey's post hoc test, $n = 4$. Error bars, S.D.

similar to the enhanced adhesion observed when eyecups are treated with ouabain, a specific inhibitor of the Na^+/K^+-ATPase (70). Ouabain-induced adhesion could be reversed by incubating eyecups in hyperosmotic solutions, suggesting that the enhanced adhesion was due to dysregulation of subretinal ion homeostasis/fluid resorption and "cellular edema" causing swelling of the RPE apical microvilli and/or rod outer segment. Although swelling of rod outer segment or apical microvilli was not detectable histologically (supplemental Figs. 2 and 6), we did observe enlarged intercellular spaces between RPE cells and around the basal infoldings (supplemental Fig. 6). These findings lend support to our hypothesis that the subretinal microenvironment is abnormal in *Cav-1* KO mice and prompted us to assess Na^+/K^+-ATPase activity.

Effect of Cav-1 Deletion on Na^+/K^+-ATPase Activity in RPE/Choroid—The activity of the α1-Na^+/K^+-ATPase in the RPE and Müller glia is critical for spatial ion buffering in the subretinal space and indirectly maintains photoreceptor excitability (reviewed in Refs. 71 and 72). Our results are consistent with the idea that loss of Cav-1 results in photoreceptor-extrinsic alterations in subretinal ion/fluid homeostasis, and Cav-1 and the α1-Na^+/K^+-ATPase colocalize in RPE and Müller glia (Fig. 1). We therefore measured Na^+/K^+-ATPase activity purified from RPE microsomes from *Cav-1* KO and control mice. We chose to prepare Na^+/K^+-ATPase from RPE instead of neural retina because 1) the apically localized α1-Na^+/K^+-ATPase regulates the $[Na^+]$ in the subretinal space around photoreceptor outer segments (72); 2) the RPE fraction contains mostly the α1 isoform, whereas the retina contains a large amount of the photoreceptor-expressed α3 isoform (73). Surprisingly, as shown in Fig. 6*A*, total Na^+/K^+-ATPase activity in RPE microsomes measured at saturating concentrations of all ligands was enhanced in Cav-1 KO microsomes, as has been recently observed in cardiac fibroblasts from *Cav-1* KO mice (74). The increased total activity in RPE could not be explained by increases in levels of Na^+/K^+-ATPase because Western blots from microsomal fractions indicated similar levels of enzyme (Fig. 6*B*). It should be noted that Na^+/K^+-ATPase functions well below V_{max} under physiological conditions (75). Therefore, we measured the activation of the enzyme by increasing concentrations of K^+ (Fig. 6*C*) or Na^+ (Fig. 6*D*). Na^+/K^+-ATPase from *Cav-1* KO RPE microsomes had a significantly reduced apparent affinity for K^+ ($K_{0.5}$ K^+ and Hill coefficients, *n*, were as follows: 1.40 ± 0.12 mM, $n = 1.5$ for *Cav-1* KO and 0.51 ± 0.11 mM, $n = 1.0$ for controls). There was no difference in the apparent affinity for Na^+ ($K_{0.5}$ Na^+ and Hill coefficients, *n*, were as follows: 5.99 ± 0.38 mM, $n = 2.2$ for *Cav-1* KO and 5.72 ± 0.46 mM, $n = 2.0$ for controls). The reduction in K^+ affinity in the physiological range of subretinal K^+ suggests that Na^+/K^+-ATPase activity may be reduced *in vivo*.

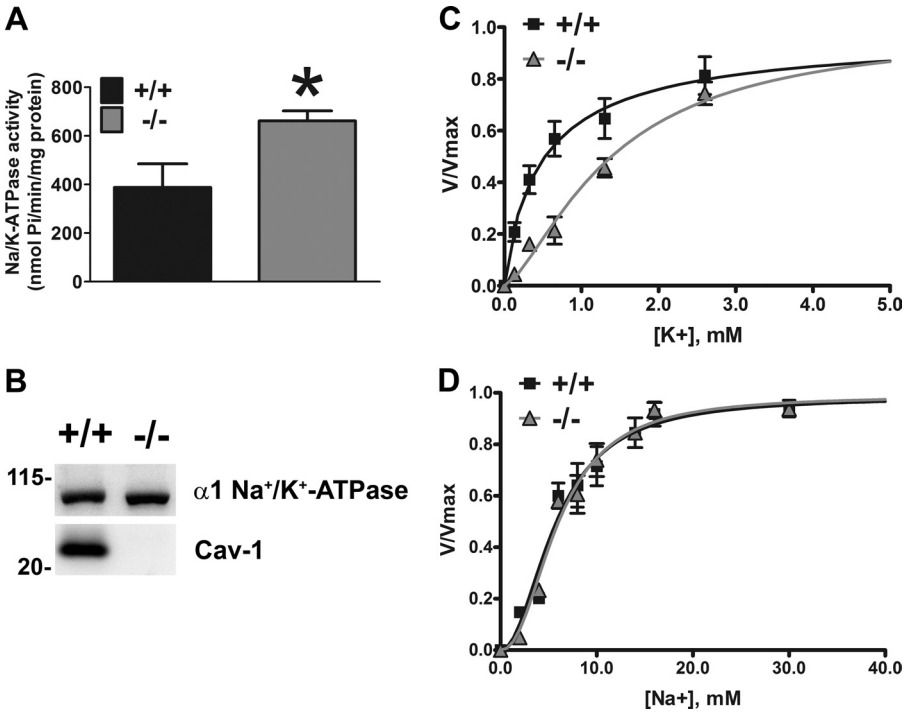

FIGURE 6. **Effect of *Cav-1* deletion on Na^+/K^+-ATPase activity.** Na^+/K^+-ATPase was partially purified from mouse eyecup microsomes and ATPase activity was measured as a function of K^+ (*A*) or Na^+ (*B*) concentration. V_{max} was determined for each preparation separately. K^+ affinity was significantly decreased in the absence of Cav-1 ($p \leq 0.05$; Student's *t* test; $n = 3$ independent microsomal preparations). Na^+ affinity was not significantly different. Error bars, S.E.

DISCUSSION

The major finding in this study is that ablation of *Cav-1* impairs retinal function due to changes in the subretinal/RPE microenvironment and not because of disturbances of the intrinsic properties of photoreceptors. Cav-1 is expressed in photoreceptors (28, 30–33), colocalizes with rhodopsin during development (76), and even has been detected in disk membranes (29). However, considering the normal function of isolated rods and the normal morphology and ultrastructure of *Cav-1* KO photoreceptors, our results suggest that photoreceptor-intrinsic Cav-1 expression does not significantly influence phototransduction or photoreceptor outer segment assembly. Future studies will focus on how *Cav-1* ablation affects retinal support cells, such as the RPE and Müller glia that control the environment in which retinal neurons reside, *in vivo*, thus indirectly impacting retinal function.

Cav-1 protein is localized to Müller glial and RPE cells and colocalizes with the α1-Na^+/K^+-ATPase (Fig. 1). Cav-1 has been identified as a Müller glia-enriched transcript compared with retinal neurons (38), and its expression increases as Müller glia mature with the same temporal expression as aquaporin-4 and the inwardly rectifying potassium channel, Kir4.1 (37). In RPE, Cav-1 and morphologically identifiable caveolae localize to both the apical membranes facing photoreceptors and the basal RPE membranes facing the choroid (35), consistent with the localization shown in Fig. 1. We note that Cav-1 immunoreactivity is also prominent in retinal and choroidal vasculature, as expected, based on several reports of Cav-1 and caveolae in retinal vascular endothelium and pericytes (40, 41, 43, 77, 78). Both Müller glial (71) and RPE (72) cells play critical roles in maintaining the retinal environment by regulating active transport properties and blood-retinal barrier functions.

Disruption of the retinal microenvironment, such as alterations in pH, ion, or fluid homeostasis, can lead to metabolic dysfunction and compromise retinal neuronal activity. Genetic ablation of the basolateral lactate transporter of the RPE, monocarboxylate transporter 3 (Mct3; slc16A8), leads to a strikingly similar ERG impairment as that found in this study, *in vivo*, and also does not affect responses recorded from isolated rods (79). Loss of Mct3 leads to extracellular accumulation of lactate and probably decreases subretinal pH. Deletion of either carbonic anhydrase XIV (80) or anion exchanger 3 (AE3/slc4A3) (81) also suppress ERG responses due to decreased extracellular pH and increased pCO_2. Furthermore, pharmacological inhibition of either lactate transport (82) or carbonic anhydrase (83) activity reduces ERG responses *in vivo*. Our MEMRI results showing reduced ion uptake in the outer retina in the dark suggest that the ERG deficit results from a suppressed dark current *in vivo*. Decreased pH is well known to depress overall retinal function (84), and protons specifically suppress the dark current in isolated rods (85). Intriguingly, these pH effects are reversible and might explain why Cav-1 deletion results in functional deficits (*i.e.* reduced dark-adapted ion uptake and ERG response) *in vivo* but normal photoreceptor function in buffered medium *in vitro*.

A central contributor to regulation of pH, ion, and fluid homeostasis in the retina is the α1 isoform of the Na^+/K^+-ATPase expressed in both the RPE and Müller glia (73). Dysregulation of ATPase activity can cause disturbances in pH, fluid, and ion homeostasis in subretinal space because the Na^+ gradient established drives myriad transport activities to regulate pH, ions, and subretinal fluid (72). Our results show significant colocalization between Cav-1 and α1-Na^+/K^+-ATPase (Fig. 1). In kidney epithelium, Cav-1 is associated with the Na^+/

K^+-ATPase (86, 87), and the α1-Na^+/K^+-ATPase contains two consensus Cav-1 binding motifs (88). In the retina, inhibition of Na^+/K^+-ATPase activity leads to depressed Mn^{2+} uptake as measured by MEMRI (52) as well as enhanced retinal adhesion that is resolvable by hyperosmotic treatment (70), two observations reproduced in *Cav-1* KO eyes. This led us to examine Na^+/K^+-ATPase activity in *Cav-1* KO RPE/choroid, and our results indicate that, within the physiological range of subretinal K^+, ATPase activity was reduced (Fig. 6). Surprisingly, V_{max} was significantly higher in *Cav-1* KO membranes, a finding recently observed in *Cav-1* KO cardiac fibroblasts (74). These results indicate that the loss of Cav-1 affects Na^+/K^+ ATPase activity, but we cannot yet determine whether this effect is due to disruption of a complex containing Cav-1 and the Na^+/K^+-ATPase or is due to indirect changes in either membrane composition or ion concentrations. Na^+/K^+-ATPase activity is exquisitely sensitive to membrane lipids, such as cholesterol (89, 90), and Cav-1 has a well established role in cholesterol trafficking (reviewed in Ref. 2). Hypertonicity can up-regulate the expression of the non-obligatory γ-subunit (FXYD2) of the Na^+/K^+-ATPase (91). It is possible that loss of Cav-1 leads to a stress response that up-regulates of FXYD family Na^+/K^+-ATPase regulators, but this remains to be determined.

In summary, our results clearly demonstrate that loss of expression of Cav-1 in photoreceptors, *per se*, is not responsible for the functional visual deficit observed. Our results suggest that loss of Cav-1 function affects ion transport activities in the RPE and possibly Müller glial cells that result in photoreceptor dysfunction. However, we cannot eliminate the contributions of other Cav-1-rich sources, such as retinal vascular cells. We are currently developing approaches to manipulate Cav-1 expression in specific retinal cells that will be useful in dissecting the contribution of specific cellular sources to the observed phenotype and will allow us to define cell-specific Cav-1 functions in the retina.

Acknowledgments—We thank Barbara Nagel and Dr. Jan Ryerse from the Saint Louis University Research and Confocal Microscopy Core for excellent electron microscopy. We also thank Mark Dittmar from the Dean McGee Eye Institute vivarium for animal care assistance.

REFERENCES

1. Cohen, A. W., Hnasko, R., Schubert, W., and Lisanti, M. P. (2004) Role of caveolae and caveolins in health and disease. *Physiol. Rev.* **84,** 1341–1379
2. Parton, R. G., and Simons, K. (2007) The multiple faces of caveolae. *Nat. Rev. Mol. Cell Biol.* **8,** 185–194
3. Boyd, N. L., Park, H., Yi, H., Boo, Y. C., Sorescu, G. P., Sykes, M., and Jo, H. (2003) Chronic shear induces caveolae formation and alters ERK and Akt responses in endothelial cells. *Am. J. Physiol. Heart Circ. Physiol.* **285,** H1113–H1122
4. Sinha, B., Köster, D., Ruez, R., Gonnord, P., Bastiani, M., Abankwa, D., Stan, R. V., Butler-Browne, G., Vedie, B., Johannes, L., Morone, N., Parton, R. G., Raposo, G., Sens, P., Lamaze, C., and Nassoy, P. (2011) Cells respond to mechanical stress by rapid disassembly of caveolae. *Cell* **144,** 402–413
5. Yu, J., Bergaya, S., Murata, T., Alp, I. F., Bauer, M. P., Lin, M. I., Drab, M., Kurzchalia, T. V., Stan, R. V., and Sessa, W. C. (2006) Direct evidence for the role of caveolin-1 and caveolae in mechanotransduction and remodeling of blood vessels. *J. Clin. Invest.* **116,** 1284–1291
6. Rothberg, K. G., Heuser, J. E., Donzell, W. C., Ying, Y. S., Glenney, J. R., and Anderson, R. G. (1992) Caveolin, a protein component of caveolae membrane coats. *Cell* **68,** 673–682
7. Scherer, P. E., Okamoto, T., Chun, M., Nishimoto, I., Lodish, H. F., and Lisanti, M. P. (1996) Identification, sequence, and expression of caveolin-2 defines a caveolin gene family. *Proc. Natl. Acad. Sci. U.S.A.* **93,** 131–135
8. Tang, Z., Scherer, P. E., Okamoto, T., Song, K., Chu, C., Kohtz, D. S., Nishimoto, I., Lodish, H. F., and Lisanti, M. P. (1996) Molecular cloning of caveolin-3, a novel member of the caveolin gene family expressed predominantly in muscle. *J. Biol. Chem.* **271,** 2255–2261
9. Way, M., and Parton, R. G. (1996) M-caveolin, a muscle-specific caveolin-related protein. *FEBS Lett.* **378,** 108–112
10. Isshiki, M., Ying, Y. S., Fujita, T., and Anderson, R. G. (2002) A molecular sensor detects signal transduction from caveolae in living cells. *J. Biol. Chem.* **277,** 43389–43398
11. Lisanti, M. P., Scherer, P. E., Vidugiriene, J., Tang, Z., Hermanowski-Vosatka, A., Tu, Y. H., Cook, R. F., and Sargiacomo, M. (1994) Characterization of caveolin-rich membrane domains isolated from an endothelial-rich source. Implications for human disease. *J. Cell Biol.* **126,** 111–126
12. Patel, H. H., Murray, F., and Insel, P. A. (2008) Caveolae as organizers of pharmacologically relevant signal transduction molecules. *Annu. Rev. Pharmacol. Toxicol.* **48,** 359–391
13. Li, S., Couet, J., and Lisanti, M. P. (1996) Src tyrosine kinases, Gα subunits, and H-Ras share a common membrane-anchored scaffolding protein, caveolin. Caveolin binding negatively regulates the auto-activation of Src tyrosine kinases. *J. Biol. Chem.* **271,** 29182–29190
14. García-Cardeña, G., Oh, P., Liu, J., Schnitzer, J. E., and Sessa, W. C. (1996) Targeting of nitric-oxide synthase to endothelial cell caveolae via palmitoylation. Implications for nitric oxide signaling. *Proc. Natl. Acad. Sci. U.S.A.* **93,** 6448–6453
15. Cao, G., Yang, G., Timme, T. L., Saika, T., Truong, L. D., Satoh, T., Goltsov, A., Park, S. H., Men, T., Kusaka, N., Tian, W., Ren, C., Wang, H., Kadmon, D., Cai, W. W., Chinault, A. C., Boone, T. B., Bradley, A., and Thompson, T. C. (2003) Disruption of the caveolin-1 gene impairs renal calcium reabsorption and leads to hypercalciuria and urolithiasis. *Am. J. Pathol.* **162,** 1241–1248
16. Drab, M., Verkade, P., Elger, M., Kasper, M., Lohn, M., Lauterbach, B., Menne, J., Lindschau, C., Mende, F., Luft, F. C., Schedl, A., Haller, H., and Kurzchalia, T. V. (2001) Loss of caveolae, vascular dysfunction, and pulmonary defects in caveolin-1 gene-disrupted mice. *Science* **293,** 2449–2452
17. Razani, B., Engelman, J. A., Wang, X. B., Schubert, W., Zhang, X. L., Marks, C. B., Macaluso, F., Russell, R. G., Li, M., Pestell, R. G., Di Vizio, D., Hou, H., Jr., Kneitz, B., Lagaud, G., Christ, G. J., Edelmann, W., and Lisanti, M. P. (2001) Caveolin-1 null mice are viable but show evidence of hyperproliferative and vascular abnormalities. *J. Biol. Chem.* **276,** 38121–38138
18. Zhao, Y. Y., Liu, Y., Stan, R. V., Fan, L., Gu, Y., Dalton, N., Chu, P. H., Peterson, K., Ross, J., Jr., and Chien, K. R. (2002) Defects in caveolin-1 cause dilated cardiomyopathy and pulmonary hypertension in knockout mice. *Proc. Natl. Acad. Sci. U.S.A.* **99,** 11375–11380
19. Schubert, W., Frank, P. G., Woodman, S. E., Hyogo, H., Cohen, D. E., Chow, C. W., and Lisanti, M. P. (2002) Microvascular hyperpermeability in caveolin-1(-/-) knock-out mice. Treatment with a specific nitric-oxide synthase inhibitor, L-NAME, restores normal microvascular permeability in Cav-1 null mice. *J. Biol. Chem.* **277,** 40091–40098
20. Cohen, A. W., Razani, B., Schubert, W., Williams, T. M., Wang, X. B., Iyengar, P., Brasaemle, D. L., Scherer, P. E., and Lisanti, M. P. (2004) Role of caveolin-1 in the modulation of lipolysis and lipid droplet formation. *Diabetes* **53,** 1261–1270
21. Fernández, M. A., Albor, C., Ingelmo-Torres, M., Nixon, S. J., Ferguson, C., Kurzchalia, T., Tebar, F., Enrich, C., Parton, R. G., and Pol, A. (2006) Caveolin-1 is essential for liver regeneration. *Science* **313,** 1628–1632
22. Cohen, A. W., Razani, B., Wang, X. B., Combs, T. P., Williams, T. M., Scherer, P. E., and Lisanti, M. P. (2003) Caveolin-1-deficient mice show insulin resistance and defective insulin receptor protein expression in adipose tissue. *Am. J. Physiol. Cell Physiol.* **285,** C222–C235
23. Klaassen, I., Hughes, J. M., Vogels, I. M., Schalkwijk, C. G., Van Noorden, C. J., and Schlingemann, R. O. (2009) Altered expression of genes related to blood-retina barrier disruption in streptozotocin-induced diabetes.

Exp. Eye Res. **89,** 4–15
24. Hauck, S. M., Dietter, J., Kramer, R. L., Hofmaier, F., Zipplies, J. K., Amann, B., Feuchtinger, A., Deeg, C. A., and Ueffing, M. (2010) Deciphering membrane-associated molecular processes in target tissue of autoimmune uveitis by label-free quantitative mass spectrometry. *Mol. Cell Proteomics* **9,** 2292–2305
25. Cao, H., Alston, L., Ruschman, J., and Hegele, R. A. (2008) Heterozygous CAV1 frameshift mutations (MIM 601047) in patients with atypical partial lipodystrophy and hypertriglyceridemia. *Lipids Health Dis.* **7,** 3
26. Thorleifsson, G., Walters, G. B., Hewitt, A. W., Masson, G., Helgason, A., DeWan, A., Sigurdsson, A., Jonasdottir, A., Gudjonsson, S. A., Magnusson, K. P., Stefansson, H., Lam, D. S., Tam, P. O., Gudmundsdottir, G. J., Southgate, L., Burdon, K. P., Gottfredsdottir, M. S., Aldred, M. A., Mitchell, P., St Clair, D., Collier, D. A., Tang, N., Sveinsson, O., Macgregor, S., Martin, N. G., Cree, A. J., Gibson, J., Macleod, A., Jacob, A., Ennis, S., Young, T. L., Chan, J. C., Karwatowski, W. S., Hammond, C. J., Thordarson, K., Zhang, M., Wadelius, C., Lotery, A. J., Trembath, R. C., Pang, C. P., Hoh, J., Craig, J. E., Kong, A., Mackey, D. A., Jonasson, F., Thorsteinsdottir, U., and Stefansson, K. (2010) Common variants near CAV1 and CAV2 are associated with primary open-angle glaucoma. *Nat. Genet.* **42,** 906–909
27. Wiggs, J. L., Kang, J. H., Yaspan, B. L., Mirel, D. B., Laurie, C., Crenshaw, A., Brodeur, W., Gogarten, S., Olson, L. M., Abdrabou, W., DelBono, E., Loomis, S., Haines, J. L., and Pasquale, L. R. (2011) Common variants near CAV1 and CAV2 are associated with primary open-angle glaucoma in Caucasians from the USA. *Hum. Mol. Genet.* **20,** 4707–4713
28. Boesze-Battaglia, K., Dispoto, J., and Kahoe, M. A. (2002) Association of a photoreceptor-specific tetraspanin protein, ROM-1, with triton X-100-resistant membrane rafts from rod outer segment disk membranes. *J. Biol. Chem.* **277,** 41843–41849
29. Corley, S. C., and Albert, A. D. (2011) Assessment of bovine rod outer segment disk membrane heterogeneity utilizing flow cytometry. *Exp. Eye Res.* **92,** 20–27
30. Elliott, M. H., Fliesler, S. J., and Ghalayini, A. J. (2003) Cholesterol-dependent association of caveolin-1 with the transducin α subunit in bovine photoreceptor rod outer segments. Disruption by cyclodextrin and guanosine 5′-*O*-(3-thiotriphosphate). *Biochemistry* **42,** 7892–7903
31. Kachi, S., Yamazaki, A., and Usukura, J. (2001) Localization of caveolin-1 in photoreceptor synaptic ribbons. *Invest Ophthalmol. Vis. Sci.* **42,** 850–852
32. Nair, K. S., Balasubramanian, N., and Slepak, V. Z. (2002) Signal-dependent translocation of transducin, RGS9–1-Gβ5L complex, and arrestin to detergent-resistant membrane rafts in photoreceptors. *Curr. Biol.* **12,** 421–425
33. Senin, I. I., Höppner-Heitmann, D., Polkovnikova, O. O., Churumova, V. A., Tikhomirova, N. K., Philippov, P. P., and Koch, K. W. (2004) Recoverin and rhodopsin kinase activity in detergent-resistant membrane rafts from rod outer segments. *J. Biol. Chem.* **279,** 48647–48653
34. Bridges, C. C., El-Sherbeny, A., Roon, P., Ola, M. S., Kekuda, R., Ganapathy, V., Camero, R. S., Cameron, P. L., and Smith, S. B. (2001) A comparison of caveolae and caveolin-1 to folate receptor α in retina and retinal pigment epithelium. *Histochem. J.* **33,** 149–158
35. Mora, R. C., Bonilha, V. L., Shin, B. C., Hu, J., Cohen-Gould, L., Bok, D., and Rodriguez-Boulan, E. (2006) Bipolar assembly of caveolae in retinal pigment epithelium. *Am. J. Physiol. Cell Physiol.* **290,** C832–C843
36. Omri, S., Behar-Cohen, F., de Kozak, Y., Sennlaub, F., Verissimo, L. M., Jonet, L., Savoldelli, M., Omri, B., and Crisanti, P. (2011) Microglia/macrophages migrate through retinal epithelium barrier by a transcellular route in diabetic retinopathy. Role of PKCζ in the Goto Kakizaki rat model. *Am. J. Pathol.* **179,** 942–953
37. Nelson, B. R., Ueki, Y., Reardon, S., Karl, M. O., Georgi, S., Hartman, B. H., Lamba, D. A., and Reh, T. A. (2011) Genome-wide analysis of Müller glial differentiation reveals a requirement for Notch signaling in postmitotic cells to maintain the glial fate. *PLoS One* **6,** e22817
38. Roesch, K., Jadhav, A. P., Trimarchi, J. M., Stadler, M. B., Roska, B., Sun, B. B., and Cepko, C. L. (2008) The transcriptome of retinal Müller glial cells. *J. Comp Neurol.* **509,** 225–238
39. Feng, Y., Venema, V. J., Venema, R. C., Tsai, N., and Caldwell, R. B. (1999) VEGF induces nuclear translocation of Flk-1/KDR, endothelial nitric-oxide synthase, and caveolin-1 in vascular endothelial cells. *Biochem. Biophys. Res. Commun.* **256,** 192–197
40. Feng, Y., Venema, V. J., Venema, R. C., Tsai, N., Behzadian, M. A., and Caldwell, R. B. (1999) VEGF-induced permeability increase is mediated by caveolae. *Invest. Ophthalmol. Vis. Sci.* **40,** 157–167
41. Stitt, A. W., Burke, G. A., Chen, F., McMullen, C. B., and Vlassara, H. (2000) Advanced glycation end-product receptor interactions on microvascular cells occur within caveolin-rich membrane domains. *FASEB J.* **14,** 2390–2392
42. Chen, W., Jump, D. B., Esselman, W. J., and Busik, J. V. (2007) Inhibition of cytokine signaling in human retinal endothelial cells through modification of caveolae/lipid rafts by docosahexaenoic acid. *Invest. Ophthalmol. Vis. Sci.* **48,** 18–26
43. Opreanu, M., Tikhonenko, M., Bozack, S., Lydic, T. A., Reid, G. E., McSorley, K. M., Sochacki, A., Perez, G. I., Esselman, W. J., Kern, T., Kolesnick, R., Grant, M. B., and Busik, J. V. (2011) The unconventional role of acid sphingomyelinase in regulation of retinal microangiopathy in diabetic human and animal models. *Diabetes* **60,** 2370–2378
44. Elliott, M. H., Nash, Z. A., Takemori, N., Fliesler, S. J., McClellan, M. E., and Naash, M. I. (2008) Differential distribution of proteins and lipids in detergent-resistant and detergent-soluble domains in rod outer segment plasma membranes and disks. *J. Neurochem.* **104,** 336–352
45. Tanito, M., Brush, R. S., Elliott, M. H., Wicker, L. D., Henry, K. R., and Anderson, R. E. (2009) High levels of retinal membrane docosahexaenoic acid increase susceptibility to stress-induced degeneration. *J. Lipid Res.* **50,** 807–819
46. Hood, D. C., and Birch, D. G. (1994) Rod phototransduction in retinitis pigmentosa. Estimation and interpretation of parameters derived from the rod *a*-wave. *Invest. Ophthalmol. Vis. Sci.* **35,** 2948–2961
47. Mandal, M. N., Moiseyev, G. P., Elliott, M. H., Kasus-Jacobi, A., Li, X., Chen, H., Zheng, L., Nikolaeva, O., Floyd, R. A., Ma, J. X., and Anderson, R. E. (2011) α-phenyl-*N*-*tert*-butylnitrone (PBN) prevents light-induced degeneration of the retina by inhibiting RPE65 protein isomerohydrolase activity. *J. Biol. Chem.* **286,** 32491–32501
48. Berkowitz, B. A., Gradianu, M., Bissig, D., Kern, T. S., and Roberts, R. (2009) Retinal ion regulation in a mouse model of diabetic retinopathy. Natural history and the effect of copper/zinc superoxide dismutase overexpression. *Invest. Ophthalmol. Vis. Sci.* **50,** 2351–2358
49. Calkins, D. J., Horner, P. J., Roberts, R., Gradianu, M., and Berkowitz, B. A. (2008) Manganese-enhanced MRI of the DBA/2J mouse model of hereditary glaucoma. *Invest. Ophthalmol. Vis. Sci.* **49,** 5083–5088
50. Berkowitz, B. A. (1996) Adult and newborn rat inner retinal oxygenation during carbogen and 100% oxygen breathing. Comparison using magnetic resonance imaging δ Po2 mapping. *Invest. Ophthalmol. Vis. Sci.* **37,** 2089–2098
51. Berkowitz, B. A., Roberts, R., Goebel, D. J., and Luan, H. (2006) Noninvasive and simultaneous imaging of layer-specific retinal functional adaptation by manganese-enhanced MRI. *Invest. Ophthalmol. Vis. Sci.* **47,** 2668–2674
52. Berkowitz, B. A., Roberts, R., Luan, H., Bissig, D., Bui, B. V., Gradianu, M., Calkins, D. J., and Vingrys, A. J. (2007) Manganese-enhanced MRI studies of alterations of intraretinal ion demand in models of ocular injury. *Invest. Ophthalmol. Vis. Sci.* **48,** 3796–3804
53. Cheng, H., Nair, G., Walker, T. A., Kim, M. K., Pardue, M. T., Thulé, P. M., Olson, D. E., and Duong, T. Q. (2006) Structural and functional MRI reveals multiple retinal layers. *Proc. Natl. Acad. Sci. U.S.A.* **103,** 17525–17530
54. Chen, C. K., Woodruff, M. L., Chen, F. S., Chen, D., and Fain, G. L. (2010) Background light produces a recoverin-dependent modulation of activated rhodopsin lifetime in mouse rods. *J. Neurosci.* **30,** 1213–1220
55. Woodruff, M. L., Janisch, K. M., Peshenko, I. V., Dizhoor, A. M., Tsang, S. H., and Fain, G. L. (2008) Modulation of phosphodiesterase 6 turn-off during background illumination in mouse rod photoreceptors. *J. Neurosci.* **28,** 2064–2074
56. Agbaga, M. P., Brush, R. S., Mandal, M. N., Henry, K., Elliott, M. H., and Anderson, R. E. (2008) Role of Stargardt-3 macular dystrophy protein (ELOVL4) in the biosynthesis of very long chain fatty acids. *Proc. Natl. Acad. Sci. U.S.A.* **105,** 12843–12848

57. Stricker, H. M., Ding, X. Q., Quiambao, A., Fliesler, S. J., and Naash, M. I. (2005) The $Cys^{214} \rightarrow Ser$ mutation in peripherin/rds causes a loss-of-function phenotype in transgenic mice. *Biochem. J.* **388,** 605–613
58. Nandrot, E. F., Anand, M., Sircar, M., and Finnemann, S. C. (2006) Novel role for $\alpha v\beta 5$-integrin in retinal adhesion and its diurnal peak. *Am. J. Physiol. Cell Physiol.* **290,** C1256–C1262
59. Forbush, B., 3rd (1983) Assay of Na,K-ATPase in plasma membrane preparations. Increasing the permeability of membrane vesicles using sodium dodecyl sulfate buffered with bovine serum albumin. *Anal. Biochem.* **128,** 159–163
60. Jorgensen, P. L. (1974) Isolation of (Na^+ plus K^+)-ATPase. *Methods Enzymol.* **32,** 277–290
61. Fiske, C. H., and Subbarow, Y. (1925) The Colorimetric Determination of Phosphorus. *J. Biol. Chem.* **66,** 375–400
62. Cariani, L., Thomas, L., Brito, J., and del Castillo, J. R. (2004) Bismuth citrate in the quantification of inorganic phosphate and its utility in the determination of membrane-bound phosphatases. *Anal. Biochem.* **324,** 79–83
63. Irreverre, F., Stone, A. L., Shichi, H., and Lewis, M. S. (1969) Biochemistry of visual pigments. I. Purification and properties of bovine rhodopsin. *J. Biol. Chem.* **244,** 529–536
64. Ding, X. Q., Fitzgerald, J. B., Matveev, A. V., McClellan, M. E., and Elliott, M. H. (2008) Functional activity of photoreceptor cyclic nucleotide-gated channels is dependent on the integrity of cholesterol- and sphingolipid-enriched membrane domains. *Biochemistry* **47,** 3677–3687
65. Martin, R. E., Elliott, M. H., Brush, R. S., and Anderson, R. E. (2005) Detailed characterization of the lipid composition of detergent-resistant membranes from photoreceptor rod outer segment membranes. *Invest. Ophthalmol. Vis. Sci.* **46,** 1147–1154
66. Lamb, T. D., and Pugh, E. N., Jr. (1992) A quantitative account of the activation steps involved in phototransduction in amphibian photoreceptors. *J. Physiol.* **449,** 719–758
67. Yau, K. W., and Hardie, R. C. (2009) Phototransduction motifs and variations. *Cell* **139,** 246–264
68. Berkowitz, B. A., Roberts, R., Oleske, D. A., Chang, M., Schafer, S., Bissig, D., and Gradianu, M. (2009) Quantitative mapping of ion channel regulation by visual cycle activity in rodent photoreceptors *in vivo*. *Invest. Ophthalmol. Vis. Sci.* **50,** 1880–1885
69. Woodruff, M. L., Wang, Z., Chung, H. Y., Redmond, T. M., Fain, G. L., and Lem, J. (2003) Spontaneous activity of opsin apoprotein is a cause of Leber congenital amaurosis. *Nat. Genet.* **35,** 158–164
70. Marmor, M. F., and Yao, X. Y. (1989) The enhancement of retinal adhesiveness by ouabain appears to involve cellular edema. *Invest. Ophthalmol. Vis. Sci.* **30,** 1511–1514
71. Bringmann, A., Pannicke, T., Grosche, J., Francke, M., Wiedemann, P., Skatchkov, S. N., Osborne, N. N., and Reichenbach, A. (2006) Müller cells in the healthy and diseased retina. *Prog. Retin. Eye Res.* **25,** 397–424
72. Strauss, O. (2005) The retinal pigment epithelium in visual function. *Physiol. Rev.* **85,** 845–881
73. Wetzel, R. K., Arystarkhova, E., and Sweadner, K. J. (1999) Cellular and subcellular specification of Na,K-ATPase α and β isoforms in the postnatal development of mouse retina. *J. Neurosci.* **19,** 9878–9889
74. Quintas, L. E., Pierre, S. V., Liu, L., Bai, Y., Liu, X., and Xie, Z. J. (2010) Alterations of Na^+/K^+-ATPase function in caveolin-1 knockout cardiac fibroblasts. *J. Mol. Cell Cardiol.* **49,** 525–531
75. Jones, D. H., Li, T. Y., Arystarkhova, E., Barr, K. J., Wetzel, R. K., Peng, J., Markham, K., Sweadner, K. J., Fong, G. H., and Kidder, G. M. (2005) Na,K-ATPase from mice lacking the γ subunit (FXYD2) exhibits altered Na^+ affinity and decreased thermal stability. *J. Biol. Chem.* **280,** 19003–19011
76. Berta, A. I., Boesze-Battaglia, K., Magyar, A., Szél, A., and Kiss, A. L. (2011) Localization of caveolin-1 and c-Src in mature and differentiating photoreceptors. Raft proteins co-distribute with rhodopsin during development. *J. Mol. Histol.* **42,** 523–533
77. Gardiner, T. A., and Archer, D. B. (1986) Does unidirectional vesicular transport occur in retinal vessels? *Br. J. Ophthalmol.* **70,** 249–254
78. Raviola, G., and Butler, J. M. (1983) Unidirectional vesicular transport mechanism in retinal vessels. *Invest. Ophthalmol. Vis. Sci.* **24,** 1465–1474
79. Daniele, L. L., Sauer, B., Gallagher, S. M., Pugh, E. N., Jr., and Philp, N. J. (2008) Altered visual function in monocarboxylate transporter 3 (Slc16a8) knockout mice. *Am. J. Physiol. Cell Physiol.* **295,** C451–C457
80. Ogilvie, J. M., Ohlemiller, K. K., Shah, G. N., Ulmasov, B., Becker, T. A., Waheed, A., Hennig, A. K., Lukasiewicz, P. D., and Sly, W. S. (2007) Carbonic anhydrase XIV deficiency produces a functional defect in the retinal light response. *Proc. Natl. Acad. Sci. U.S.A.* **104,** 8514–8519
81. Alvarez, B. V., Gilmour, G. S., Mema, S. C., Martin, B. T., Shull, G. E., Casey, J. R., and Sauvé, Y. (2007) Blindness caused by deficiency in AE3 chloride/bicarbonate exchanger. *PLoS. One.* **2,** e839
82. Bui, B. V., Kalloniatis, M., and Vingrys, A. J. (2004) Retinal function loss after monocarboxylate transport inhibition. *Invest Ophthalmol. Vis. Sci.* **45,** 584–593
83. Findl, O., Hansen, R. M., and Fulton, A. B. (1995) The effects of acetazolamide on the electroretinographic responses in rats. *Invest. Ophthalmol. Vis. Sci.* **36,** 1019–1026
84. Niemeyer, G., and Steinberg, R. H. (1984) Differential effects of pCO_2 and pH on the ERG and light peak of the perfused cat eye. *Vision Res.* **24,** 275–280
85. Liebman, P. A., Mueller, P., and Pugh, E. N., Jr. (1984) Protons suppress the dark current of frog retinal rods. *J. Physiol.* **347,** 85–110
86. Chen, Y., Cai, T., Wang, H., Li, Z., Loreaux, E., Lingrel, J. B, and Xie, Z. (2009) Regulation of intracellular cholesterol distribution by Na/K-ATPase. *J. Biol. Chem.* **284,** 14881–14890
87. Liu, L., Ivanov, A. V., Gable, M. E., Jolivel, F., Morrill, G. A., and Askari, A. (2011) Comparative properties of caveolar and noncaveolar preparations of kidney Na^+/K^+-ATPase. *Biochemistry* **50,** 8664–8673
88. Wang, H., Haas, M., Liang, M., Cai, T., Tian, J., Li, S., and Xie, Z. (2004) Ouabain assembles signaling cascades through the caveolar Na^+/K^+-ATPase. *J. Biol. Chem.* **279,** 17250–17259
89. Yeagle, P. L. (1983) Cholesterol modulation of ($Na^+ + K^+$)-ATPase ATP hydrolyzing activity in the human erythrocyte. *Biochim. Biophys. Acta* **727,** 39–44
90. Cornelius, F., Turner, N., and Christensen, H. R. (2003) Modulation of Na,K-ATPase by phospholipids and cholesterol. II. Steady-state and presteady-state kinetics. *Biochemistry* **42,** 8541–8549
91. Wetzel, R. K., Pascoa, J. L., and Arystarkhova, E. (2004) Stress-induced expression of the γ subunit (FXYD2) modulates Na,K-ATPase activity and cell growth. *J. Biol. Chem.* **279,** 41750–41757